J. Fluid Mech. (1989), *vol.* 199, *pp.* 377–401
Printed in Great Britain

Selective withdrawal and spin-up of a rotating stratified fluid

By S. G. MONISMITH† AND T. MAXWORTHY‡

† Environmental Fluid Mechanics Laboratory, Department of Civil Engineering, Stanford University, Stanford, CA 94305-4020, USA

‡ Departments of Mechanical and Aerospace Engineering, University of Southern California, University Park, Los Angeles, CA 90089-1453, USA

(Received 18 November 1987 and in revised form 22 June 1988)

We present an experimental study demonstrating that rotation has a pronounced effect on currents induced by selective withdrawal of fluid from a density-stratified reservoir. Our observations show that initiating outflow from the reservoir generates Kelvin shear waves. These waves propagate cyclonically around the perimeter of the reservoir, establishing an anticyclonic withdrawal-layer flow. This flow accelerates owing to the production of relative vorticity by compression of 'planetary' vorticity. The withdrawal-layer thickness as shown by vertical profiles of the horizontal velocity grows with time. Separation of the side-wall boundary layers in the corners of the tank causes the spun-up flow to eventually break up into a series of counter-rotating gyres. We also present a model that describes many features of the spin-up process observed before onset of separation and subsequent gyre formation. The model shows that vertical diffusion of vorticity plays an important role in the spin-up process, leading us to conclude that apparent thickening of the withdrawal layer over time, as seen in changes in the velocity profile, is associated with the vertical diffusion of the spun-up vorticity.

1. Introduction and background

The presence of a stable density stratification in storage reservoirs means that water withdrawn at a particular elevation comes primarily from those strata closest to the level of the sink. Selective withdrawal is well known to engineers, who often make use of this phenomenon in the design of offtakes in order to optimize the quality of stored and released waters. Suitable design criteria (see Imberger 1980) have been derived mainly from experiments and theory concerned with withdrawal-layer dynamics in the absence of rotation. The neglect of rotation, at least for small and medium-size reservoirs, is frequently justified using the argument that most reservoir basins are too narrow for rotational effects to be important (see Patterson, Hamblin & Imberger 1984). However, simple scaling arguments such as those advanced by Imberger & Hamblin (1982) suggest that this may not always be the case.

Some attention has previously been devoted to the effects of rotation on selective withdrawal. Whitehead (1980) and Kranenburg (1980) studied axisymmetric, linearly stratified and layered flows into centrally located offtakes (sinks). Whitehead's theory suggested that fluid flowing inwards towards the sink would develop an appreciable amount of swirl, which would force the radial pressure gradient to strengthen with time and thus cause the withdrawal layer to thicken.

However, his quasi-steady, inviscid theory did not explain how the swirl would actually evolve; instead, he assumed that the azimuthal velocity distribution would be that of a steady, source–sink pair. In contrast, Kranenburg (1980) analysed in detail the transient flow for the case of two layers of different density. Unfortunately, the prominent role played by bottom and interfacial Ekman layers in determining this flow's development prohibits application of his results to the case of a continuous stratification, because a continuous stratification tends to suppress Ekman suction (Greenspan 1968). However, he did study the flow resulting from withdrawal from an homogeneous layer overlying a stratified region, and found that the stratified region 'spun-up', i.e. developed swirl, owing to vertical diffusion of vorticity from the homogeneous region.

It is clear from Kranenburg's work, as well as that of many others (e.g. Gill 1976, 1982), that steady flows in which Coriolis forces are important cannot be properly analysed without considering how they are established. In this paper we shall focus upon the establishment and evolution of the flow of a linearly stratified fluid into a point sink situated on one wall of a rectangular reservoir. In the next section we shall present a qualitative theory outlining how rotation can affect selective withdrawal. This qualitative theory provides a framework for understanding the experimental results presented in §4. In §5 we provide a more refined theory describing the long-term spin-up of the withdrawal flow that we observed in our experiments. Finally, we discuss and summarize our results in §6.

2. A description of selective withdrawal in a rotating fluid

2.1. *Internal wave dynamics and flow establishment*

Gill's (1976) analysis of gravitational adjustment in a rotating channel shows that rigorous analysis of the establishment of selective withdrawal in a rotating fluid is a difficult task. However, we can obtain a qualitative description of the effect of rotation on selective withdrawal by using Gill's results to understand how rotation might modify the waves that establish the withdrawal layer in the absence of rotation (Imberger, Thompson & Fandry 1976), and thereby alter the structure of the withdrawal flow as a whole.

When stratified fluid starts to flow into a sink, a withdrawal layer of limited vertical extent forms near the sink, generating internal waves (known as shear waves) which alter the potential flow field away from the sink so that it matches that at the sink (Pao & Kao 1974). Shear waves travel at the appropriate long-wave speed; in a linearly stratified fluid of depth H and buoyancy frequency N, the nth mode (i.e. the one having n velocity nodes) travels at a speed, C_n, given by Pao & Kao (1974) as

$$C_n = NH\,(n\pi)^{-1}. \tag{1}$$

Details of the establishment of the withdrawal layer and the hierarchy of dynamic balances possible are described by Imberger *et al.* (1976), who present a successful classification scheme, based largely on shear-wave dynamics, which is valid for line sinks.

Lawrence (1980) (see also Ivey & Blake 1985) extended Imberger *et al.*'s analysis to account for the case of axisymmetric withdrawal through a point sink. According to Lawrence, an inertial layer carrying a volume flux Q will reach a thickness

$$\delta = O(Q^{\frac{1}{3}}N^{-\frac{1}{3}}). \tag{2}$$

at a distance X from the sink at a time T_w such that

$$NT_w = O(X\delta^{-1}), \tag{3}$$

i.e. T_w is the time required for a wave with vertical wavelength δ to reach X. Spigel & Farrant (1984) found that (2) is valid for point sinks in channel-like reservoirs (rather than cylinders) when $\delta < B$, the width of the reservoir. According to (2) and (3), the time required to initially establish the layer near the sink is $O(N^{-1})$. If, as in most natural situations, $N \gg f$ (f is the Coriolis parameter), the withdrawal layer is established before rotation can influence the flow: consequently δ will initially be independent of f.

As the shear waves generated by initiating the flow propagate away from the sink, they must be modified by rotation. The influence of rotation on the nth-mode shear wave is determined by the magnitude of the Rossby radius of that mode (Gill 1976)

$$R_n = C_n f^{-1} \tag{4}$$

relative to the width of the reservoir, B. As shown by Gill, if $(R_n B^{-1}) > 1$, rotation has little effect on the wave front or the flow which the wave sets up. On the other hand, Gill's analysis (as applied to the problem at hand) also shows that if $(R_n B^{-1}) < 1$, the front is composed of both a continuous spectrum of dispersive Poincaré waves which travel at speeds less than C_n, and a single, non-dispersive Kelvin wave, which travels at a speed equal to C_n.

The velocity field associated with a Kelvin wave decays exponentially (with an e-folding length equal to R_n) across the channel. As sketched in figure 1, if the velocity at the wall $Y = 0$ is $U_n(Y)$, the velocity field induced by the Kelvin wave is

$$U(Z, Y) = U_n(Y)\exp(-YR_n^{-1}). \tag{5}$$

Gill found that after the passage of the initial wave front, the steady flow took the same form as the Kelvin-wave part of the wave front; implying that when $(R_n B^{-1}) \ll 1$, the steady flow is confined to a narrow coastal jet of width $O(R_n)$. Moreover, since the Kelvin wave propagates with the wall on its *right* for $f > 0$ (looking in the direction the wave is moving), the flow towards the sink develops with the wall on its *left*, i.e. is anticyclonic, rather than cyclonic as has been found for rotating gravity currents (e.g. Maxworthy 1983). Since $(\delta/H) \ll 1$, several shear-wave modes will probably be generated (Imberger *et al.* 1976); consequently the flow observed at any level will be a superposition of flows having different Rossby radii, because $(C_n/NH) \sim n^{-1}$ and hence $R_n \sim n^{-1}$. Thus we surmise that while a selective withdrawal flow might not exhibit the clear coastal jet seen for a single mode, it may still exhibit considerable lateral variation in the withdrawal-induced flow.

Since the shear wave determining the final withdrawal-layer thickness has a phase speed of $N\delta$, a parameter expressing the importance of rotation to selective withdrawal is the Burger number,

$$S = N\delta(fB)^{-1}. \tag{6}$$

Based on the preceding discussion, when $S \ll 1$ we expect large cross-channel variations in the horizontal flow, whereas when $S \gg 1$, rotation should not affect the flow. However, because the order-of-magnitude argument leading to (6) is approximate, conditions leading to values of S in excess of 1 may result in flows that are significantly influenced by rotation.

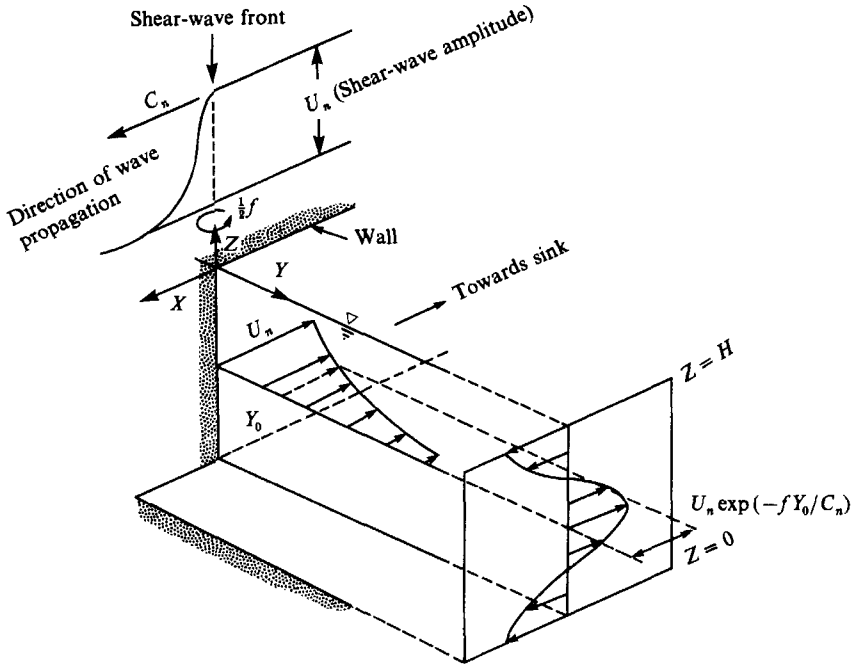

FIGURE 1. A sketch showing the spatial structure of a Kelvin shear wave.

2.2. *Flow spin-up*

The arguments outlined above suggest that the selective withdrawal flow observed in the absence of rotation can also tell us a great deal about the creation of relative vorticity by vortex compression in the presence of rotation (Kranenburg 1980). In the absence of rotation, the vertical velocity is approximately independent of X and Y, the horizontal coordinates (except near the sink) so that (for Z positive upwards)

$$\partial_Z W \sim -(Q/A\delta) \tag{7}$$

in the withdrawal layer, and zero above and below the withdrawal layer (Spigel & Farrant 1984). Here, A is the surface area of the reservoir and the subscript Z refers to differentiation with respect to Z, the vertical coordinate. Equating the rate of change of relative vertical vorticity with its production by compression of planetary vortex filaments gives

$$\partial_T \zeta \sim f \partial_Z W, \tag{8}$$

where $\zeta = \partial_X V - \partial_Y U$. Thus if (7) were valid for rotating fluids, we would estimate that by the time

$$T \sim T_\delta = (A\delta/Q), \tag{9}$$

the time required to empty the withdrawal layer, $\zeta \sim f$. A better model of this process is one that includes the vertical diffusion of vorticity, the advection of low-vorticity fluid from above, and the reduction of vortex compression as ζ approaches f. These factors will all tend to keep ζ somewhat smaller than f. Such a one-dimensional model is pursued in §5.

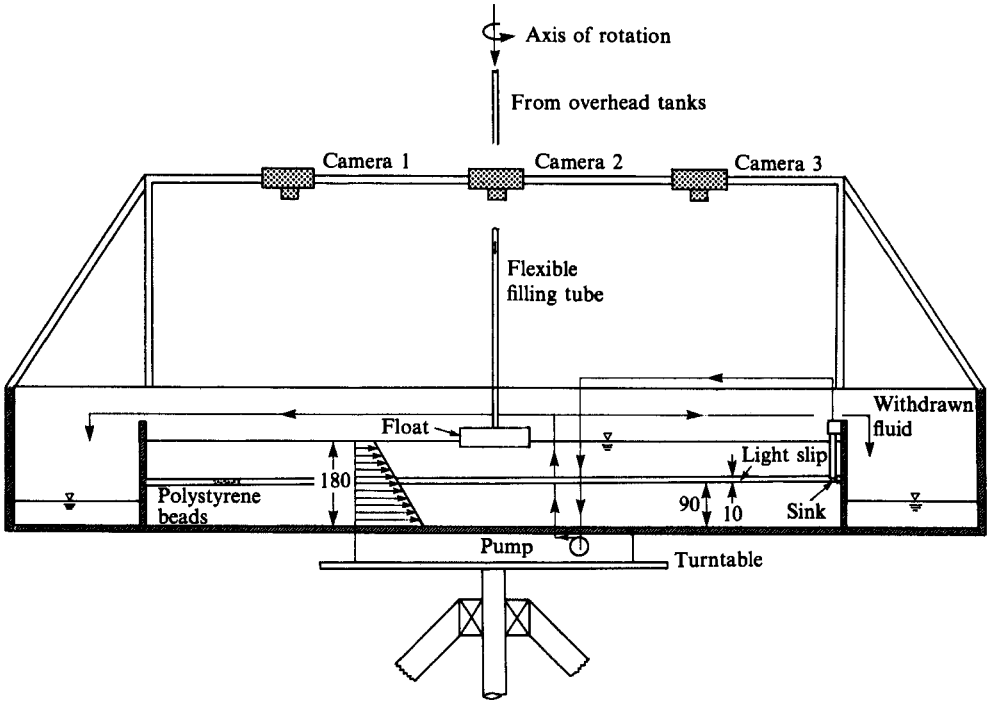

FIGURE 2. A sketch of the experimental apparatus. Note that the sink is shown in one of the three locations used in the study, and that the lighting configuration is that used in experiments 1–9.

2.3. *Summary*

The discussion above presents two conclusions which we tested experimentally: (i) the flow will be initially established by Kelvin waves and will therefore be anticyclonic; (ii) over a time proportional to T_s, vertical divergence of the vertical velocity will generate anticyclonic vorticity of order of magnitude f.

3. Experimental apparatus and procedures

All of the experiments were performed in a rectangular channel mounted on a rotating table (figure 2) described in Maxworthy (1983). The test section (dimensions: 3.24 m long; 0.58 m wide) was located in the centre of a longer tank so that the two outer sections of the tank could be used to store fluid withdrawn from the test section. In one experiment, exp. 13, a false wall was placed along the centreline of the channel running from the wall at $X = 0$ to within 290 mm of the wall at $X = L$. This was done to obtain a value of $S > 1$, while maintaining a stable rate of rotation of the table.

Two offtakes were used in the experiments. The first, used in experiments 1–9, was a pipe mounted approximately 10 mm from the wall with its open end approximately 90 mm above the bottom of the channel. The section was a section of 6 mm tubing with an elbow attached at its end such that the centreline of opening of the elbow was 90 mm above the bottom. The offtakes were attached to the side of the tank at $(X, Y) = (0.5L, B)$ in experiments 1–6, at $(X, Y) = (0, 0.5B)$ in experiments 7–9,

and at $(X, Y) = (0.08L, 0)$ in experiments 10–13. Water was drawn through the offtakes using a small pump.

The withdrawal flow was recorded using bead-streak photography (Maxworthy & Browand 1975). Because of the difficulties involved in recording the full three-dimensional structure of the flow, we used two lighting arrangements. In experiments 1–9 we concentrated on measuring the flow field in a single horizontal plane. A slit of light 10 mm high, centred 90 mm above the bottom of the channel and covering the length and breadth of the test section, illuminated neutrally buoyant polystyrene beads (specific gravity = 1.04) suspended in the fluid. The position of the slit was chosen so as to coincide with the open end of the withdrawal pipe, which we thought would be at the same level as the centre of the withdrawal layer. In the experiments, however, the withdrawal layer formed approximately 5–10 mm below the end of the pipe. Two, and in some experiments three, 35 mm cameras, each covering roughly 40% of the channel (with overlapping fields of view), were mounted on a frame approximately 1 m above the channel.

In order to obtain information about both horizontal and vertical structure of the withdrawal flow, we performed four experiments (10–13) using both an horizontal and a vertical light slit. The horizontal slit (again centred 90 mm above the bottom) illuminated the centre third of the tank, whereas the vertical plane covered a region approximately 200 cm^2 in area centred 240 mm upstream (towards increasing X) of the sink and at mid-depth. The vertical and horizontal slits did not overlap. Two cameras were used with this lighting arrangement. In order to place beads at all depths, we prepared beads of various densities by boiling the raw, unexpanded beads in a saucepan (see Silvester 1978).

After the tank was set in counterclockwise rotation at the desired speed, it was slowly filled, via a surface float, to a depth of 180 mm with linearly stratified fluid such that the density at mid-depth (the level of the light slit) was approximately that of the polystyrene beads used in recording the flow patterns. The vertical density profiles were measured by drawing off samples through holes drilled in the size of the channel and measuring each sample's density using a calibrated refractometer.

Despite the care taken in filling the tank, the fluid had not usually reached a state of solid-body rotation when filling was complete; as seen in studies of spin-up (e.g. Buznya & Veronis 1971) the time required to achieve total spin-up, i.e. the absence of relative motions, is the diffusive timescale (H^2/ν), ~ 10 h in our tank. For experiments 1–7, we generally waited 4 to 6 h after filling the tank before starting an experiment. We lengthened this period to approximately 18–24 h for the other experiments (8–13). Even then some relative motions remained. The deviation from solid-body rotation usually took the form of a set of 3 major clockwise circular vortices, approximately equal in diameter to the width of the channel, each having vertical vorticity roughly equal to 1–2% of f; i.e. the initial conditions were within 1–2% of solid-body rotation. In the experiment with the worst initial conditions, exp. 7, the residual vorticity was 2.5% of f. In contrast, for the 'best case', exp. 9, in which the fluid was allowed 18 h to spin-up before the experiment was begun, the residual vorticity was 1.4% of f.

Each experiment consisted of starting the pump and then recording bead-streak images as the flow evolved. A summary of the experimental variables such as N, f and Q are shown in table 1.

Exp.	Q (cm^3/s)	N (s^{-1})	f (s^{-1})	δ (cm)	S	T_δ (s)	Re	T_e/T_δ	Ro_Q	Remarks
1	52	1.3	0.09	3.2	0.60	1190	0.85	0.99	0.050	
3	32	1.3	0.13	2.5	0.35	1520	0.41	1.45	0.027	
4	229	1.2	0.23	5.0	0.35	424	5.89	1.51	0.055	
5	17	1.2	0.23	2.4	0.15	2740	0.20	0.97	0.009	
6	9	1.0	0.04	1.8	0.60	3930	0.08	0.78	0.035	
7	24	0.9	0.23	2.3	0.13	1860	0.28	1.39	0.013	(see text)
8	23	0.9	0.12	2.3	0.25	1940	0.27	2.26	0.023	
9	18	1.0	0.07	2.0	0.40	2160	0.19	1.97	0.036	
10	22	1.2	0.08	2.6	0.64	2220	0.30	1.43	0.030	
11	22	1.3	0.22	2.6	0.25	2220	0.30	0.74	0.030	
12	22	1.2	0.04	2.6	1.33	2220	0.30	1.49	0.030	Unstable rotation rate
13	22	1.3	0.09	2.6	1.25	2220	0.30	1.23	0.030	$B = 290$ mm

TABLE 1. Experimental parameters. $\delta = 1.0(Q/N)^{\frac{1}{3}}$; Re defined by (13); T_e = length of experiment. Ro_Q defined by (24).

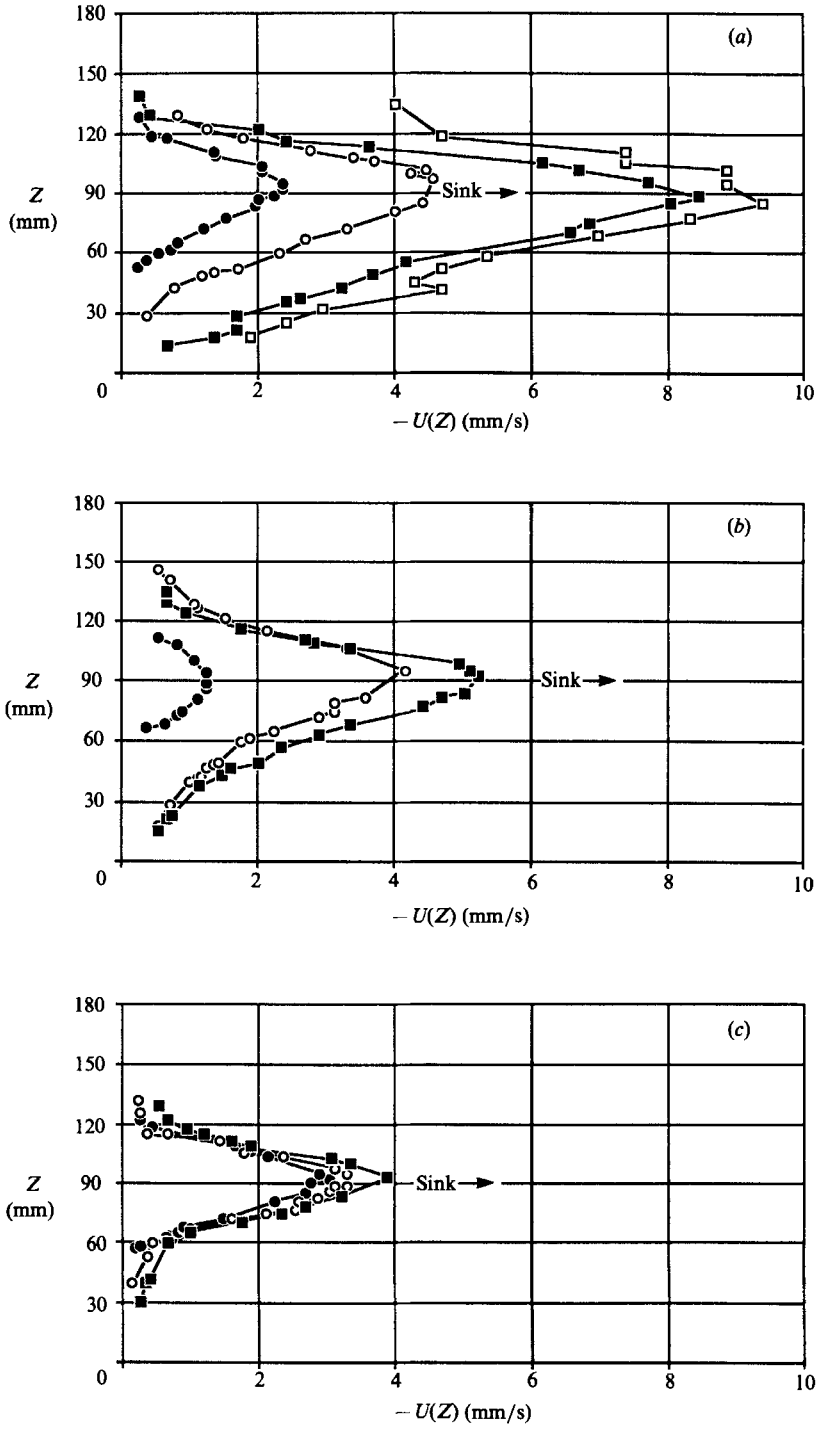

FIGURE 3. Vertical velocity profiles measured in: (*a*) exp. 11 ($S = 0.25$) at $T = 60$ s (●), 600 s (○), 1650 s (■), 2805 s (□); (*b*) exp. 10 ($S = 0.6$) at $T = 30$ s (●), 1000 s (○), 3000 s (■); and, (*c*) exp. 13 ($S = 1.25$) at $T = 60$ s (●), 960 s (○), 2700 s (■). In all three experiments $T_s = 3245$ s.

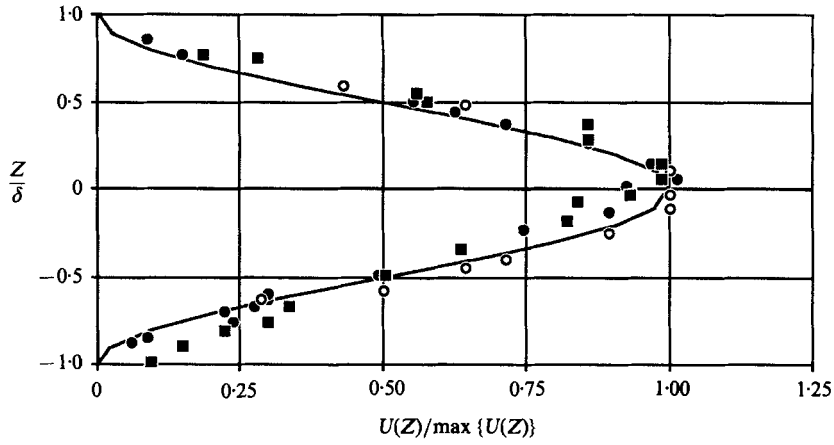

FIGURE 4. Dimensionless withdrawal-layer velocity profiles measured in exp. 11 (■), exp. 10 (○), and exp. 13 (●). These are the earliest profile from each of the set of profiles given in figure 3. The peak velocity measured in each profile and a withdrawal-layer thickness of 38 mm were used to normalize the various profiles.

4. Results

4.1. *Vertical structure of the withdrawal flow*

The withdrawal layer that formed after the pump was started can be seen in figure 3(*a–c*), plots of the vertical distribution of the horizontal velocity, as measured 240 mm upstream of the sink and 100 mm off the wall, in three experiments (10, 11 and 13) at various times. At the lowest value of S (exp. 11, figure 3*a*), there appears to be a considerable acceleration and thickening of the withdrawal flow. Flow acceleration and layer thickening are also evident in figure 3(*c*) (exp. 13, $S = 1.3$), although less so than in figure 3(*a*). Figures 3(*a*) and 3(*b*) both show velocity profiles that became asymmetric as each experiment proceeded. This asymmetry came about because the no-slip bottom remained at a fixed distance below the sink while the distance between the (effectively no-slip) free surface and the sink decreased as water was withdrawn from the tank. This point will be discussed more fully in §5.2.

The earliest profiles in figure 3(*a–c*) are replotted in figure 4, to show the initial structure of the withdrawal layer in all three experiments. In each case, these were taken approximately 60 s after the pump was switched on. In this figure, we have normalized each velocity distribution by its maximum velocity. The dimensionless vertical distance has been calculated relative to the level of the sink, and has been scaled (for all three profiles) by an apparent withdrawal-layer half-thickness of 37.5 mm, rather by the estimated thickness of 25.7 mm (table 1). This value was obtained by fitting the observed profiles to the cosine-bell distribution given in Spigel & Farrant (1984) (among others). As seen in figure 4, the scaled data, which include a factor of 4 variation in S, fit the theoretical profile reasonably well with one explainable exception: the profile from exp. 11 shows a withdrawal layer that is thicker below the sink than above. This can be attributed to the fact that N above the sink was larger than N below the sink (by approximately 14 %), because in a fluid having a vertically varying N, thicker withdrawal layers are found where N is smaller (Imberger *et al.* 1976). We shall present further discussion of withdrawal-layer thickness later.

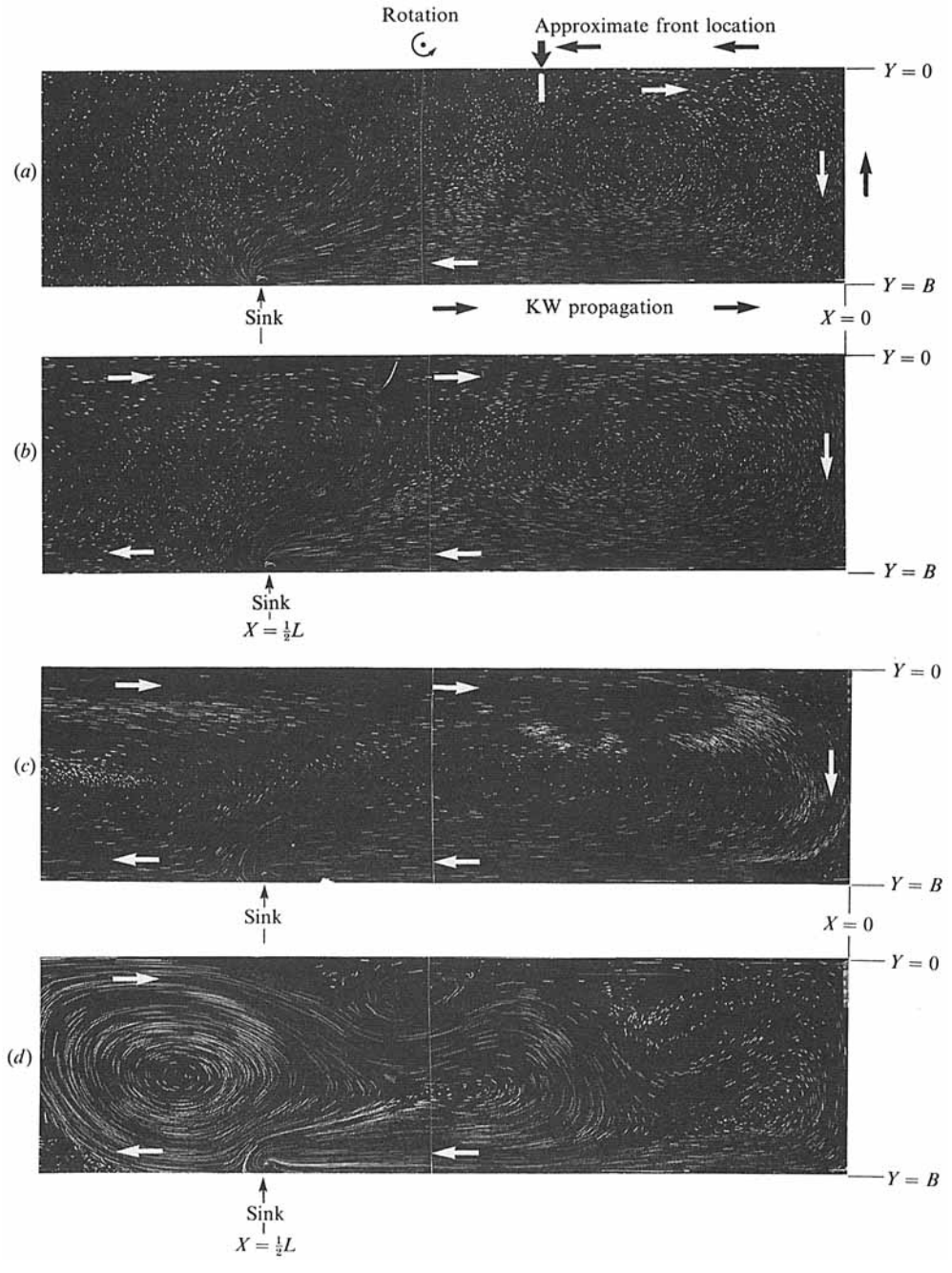

FIGURE 5. Flow patterns in exp. 3 ($S = 0.35$) at (*a*) $T = 75$ s, (*b*) 225 s, (*c*) 1065 s, (*d*) 2600 s. Approximately $\frac{2}{3}$ of tank is shown. The white arrows mark the direction of flow whereas the black arrows indicate the direction of wave propagation. In this experiment, $T_\delta = 1520$ s.

4.2. *Horizontal structure of the withdrawal flow*

The general evolution of the flow after the pump was started is shown in figure 5 which is a sequence of photos taken during exp. 3 ($S = 0.35$). This sequence typifies the experimental observations since it illustrates most of the effects of rotation on selective withdrawal found in this study: set-up of the flow by Kelvin shear waves, spin-up of a recirculating flow, and the breakdown of the flow into smaller gyres.

In the first photo, figure 5(*a*), (a 10 s exposure taken at $T \approx 75$ s after the pump had started) the clockwise withdrawal current extends upstream from the sink; it is strongest near the lower wall and decays as the opposite wall is approached. As suggested by Gill's (1976) analysis, the withdrawal flow is anticyclonic (in this case clockwise).

The low-speed region immediately above and to the right of the sink, and on the opposite wall, indicates the presence of the Kelvin-shear-wave front located at $X \approx$ 60–80 cm (the flow immediately above the sink on the opposite wall is due to a vortex remaining from the filling process). Because the sink is located near mid-depth, even-mode shear waves should dominate the unsteady response (Imberger *et al.* 1976). Using (1), we calculate that the lowest even-mode (the fastest mode with $C_2 = 3.72$ cm/s and $R_2 = 29$ cm) Kelvin-shear-wave front should have travelled approximately this distance (allowing 30 cm of propagation path for the wall at $X = 0$) in the 75 s between the time the pump was started and the time figure 5(*a*) was taken. Whereas figure 5(*a*), taken at $T \approx 155$ s, shows no withdrawal current to the left of the sink, figure 5(*b*), taken at $T \approx 225$ s, shows the withdrawal current (which flows towards increasing X) on the left side of the sink ($X > \frac{1}{2}L$) on the wall $Y = B$. Since the lowest-mode Kelvin wave generated when the pump was started should not have returned to the sink until $T \approx 190$ s, these observations support the hypothesis that the withdrawal layer is set up by Kelvin waves propagating cyclonically (counterclockwise) around the basin.

Figure 5(*c*), taken at $T \approx 1065$ s, shows an intensification (spin-up) with time of the clockwise circulation. As a consequence of this strengthening of the flow, 10–20% of the flow to the right of the sink bypasses it entirely. A small region of counterclockwise flow, bounded on the left by a stagnation point on the wall, exists around the sink itself. Figure 5(*d*), taken at $T \approx 2600$ s (a 20 s exposure), shows a substantial change in the overall flow pattern over the course of the experiment: the main clockwise gyre has split into several smaller gyres, including two weak counterclockwise gyres interposed between three clockwise gyres.

The general dependence of the shape of the flow on S can be seen in figure 6, photos taken at $T = 540$ s ($T/T_\delta = 0.20$, 20 s exposure) in exp. 5 ($S = 0.15$), at $T = 690$ s ($T/T_\delta = 0.19$, 30 s exposure) in exp. 6 ($S = 0.6$), and at $T = 420$ s ($T/T_\delta = 0.2$, 15 s exposure) in exp. 13 ($S = 1.25$). First, figure 6 shows that the flows observed at $S = 0.15$ and at $S = 0.60$ are qualitatively similar to that observed at $S = 0.35$ (figure 5), i.e. a clockwise-rotating mean flow. At $S = 1.25$, the flow is still unidirectional (i.e. towards the sink), although there is considerable shear. The relatively small value of S in exp. 5 (figure 6*a*) is accompanied by a narrower withdrawal flow embedded in a relatively stronger recirculating flow than is observed at a similar time in experiments with larger values of S (exp. 3, figure 5 and exp. 6, figure 6*b*).

The effect of sink location on the flow can be seen by comparing figures 5, 6(*a*) and 6(*b*) with figure 7: images of flows in exp. 9 ($S = 0.40$) recorded at $T = 300$ s (figure 7*a*) and $T = 3600$ s (figure 7*b*). In this experiment, the sink was located at one end of the tank rather than in the middle. Clearly there is little qualitative difference

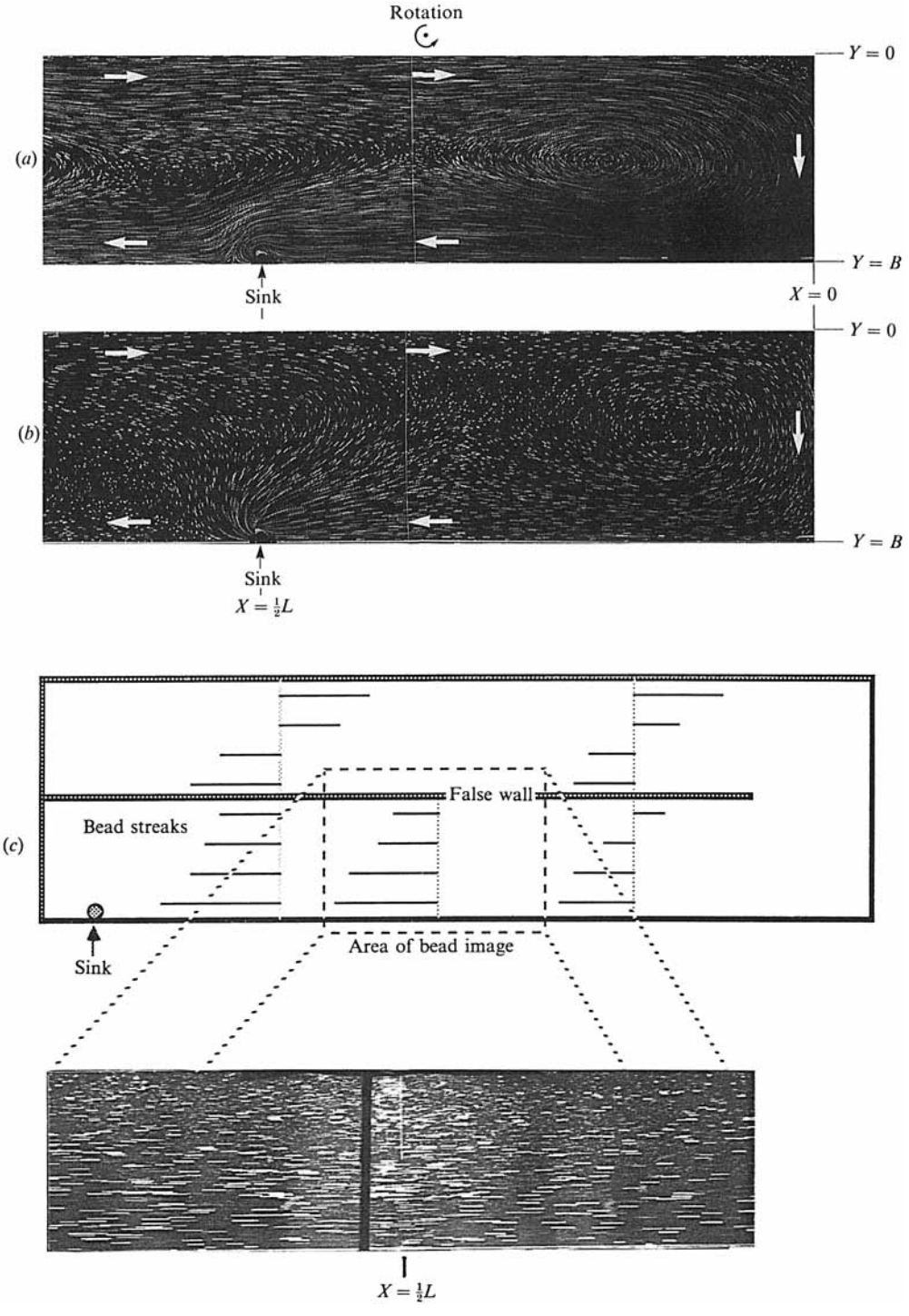

FIGURE 6. Flow patterns at $(T/T_s) \approx 0.2$ in (*a*) exp. 5 ($S = 0.15$), (*b*) exp. 6 ($S = 0.6$), and (*c*) exp. 13 ($S = 1.25$). Note that the region shown in the photo in (*c*) is only half as wide as that shown in (*a*) and (*b*), and that the sink is not shown (it was further to the left on the wall at the bottom of the photo). To place this image in proper context, we have sketched streaklines in areas of the flow that were not photographed.

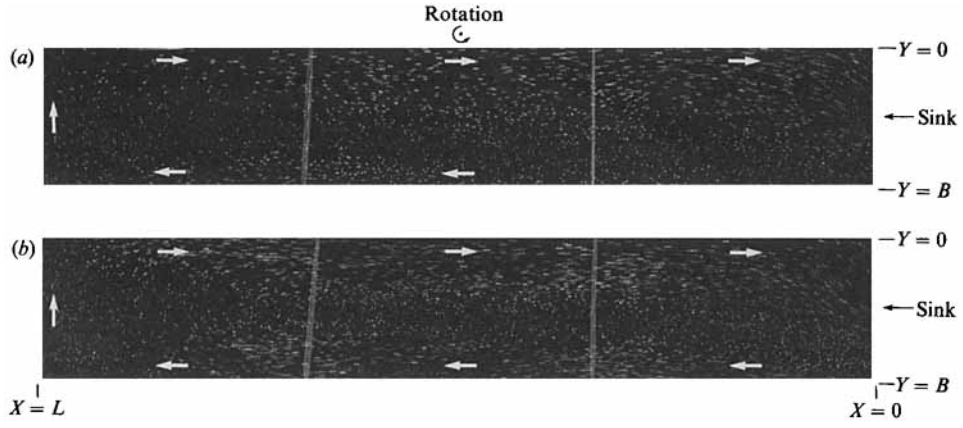

FIGURE 7. Flow patterns in exp. 9 ($S = 0.4$) at (*a*) $T = 300$ s and (*b*) 3600 s. In this experiment, $T_s = 2160$ s.

between the flows seen in figure 7 and those seen in figures 5 or 6 (i.e. before the onset of any instability).

A more detailed picture of the spin-up of the withdrawal-layer flow is given in figure 8(*a*), which plots velocity profiles $U(Y)$ at $X = \frac{1}{2}L$ for five different times during exp. 9. The initial profile in figure 8(*a*) was taken after the lowest even-mode ($R_2 = 42$ cm) Kelvin shear wave generated when the pump was started had passed the line $X = \frac{1}{2}L$. This profile shows a decay of U with distance from the wall at $Y = 0$. While this decay is similar to that which characterises a single Kelvin wave, it is not identical to that which would have been produced by the lowest even-mode Kelvin wave, as the observed profile is nearly linear (aside from the sidewall boundary layer) whereas the theoretical distribution gives an exponential decay with Y (cf. (5)). The reason for this discrepancy is unclear. As the experiment proceeded, the sidewall boundary layers grew and a nearly constant-shear flow developed. The average value of this shear flow represents the net sinkward flow. This sinkward flow is generally weaker than the superimposed shear flow: in the last profile in figure 8(*a*) the average velocity is approximately 0.5 mm/s, whereas the maximum negative velocities are nearly 3 mm/s.

All the profiles shown in figure 8(*a*) show an approximately linear variation in U across the channel (away from the two sidewall boundary layers). Since ζ, the vertical vorticity, is almost exactly equal to $-\partial_Y U$, the nearly linear shear indicates that there is virtually no transverse variation in ζ. In addition, as indicated by figure 8(*b*, *c*), plots of $U(Y)$ at six different values of X at $T = 300$ s and at $T = 3600$ s, there is little longitudinal variation, except near the endwalls, in $\partial_Y U$ and hence in ζ.

In figure 9 we plot $U(Y)$ at different times in exp. 13 ($S = 1.25$) at $X = \frac{1}{4}L$. In this sequence, the flow is directed towards the sink for all values of $Y < 30$ cm (note that $Y > 30$ cm is on the far side of the barrier which we used to divide the tank in half – see §3). Like figure 8, however, figure 9 shows a growth over time of a linear shear in the withdrawal flow. At this station, the sheared flow is not sufficiently strong to cause a flow reversal like that seen in figure 8. However, as sketched in figure 6(*c*), the flow did reverse directions approximately 2500 mm from the sink (i.e. out of the camera's field of view).

While the main body of the flows seen in both figures 8 and 9 has negative vorticity ($\sim -0.1f$ to $-0.2f$), the sidewall boundary layers possess strong positive vorticity.

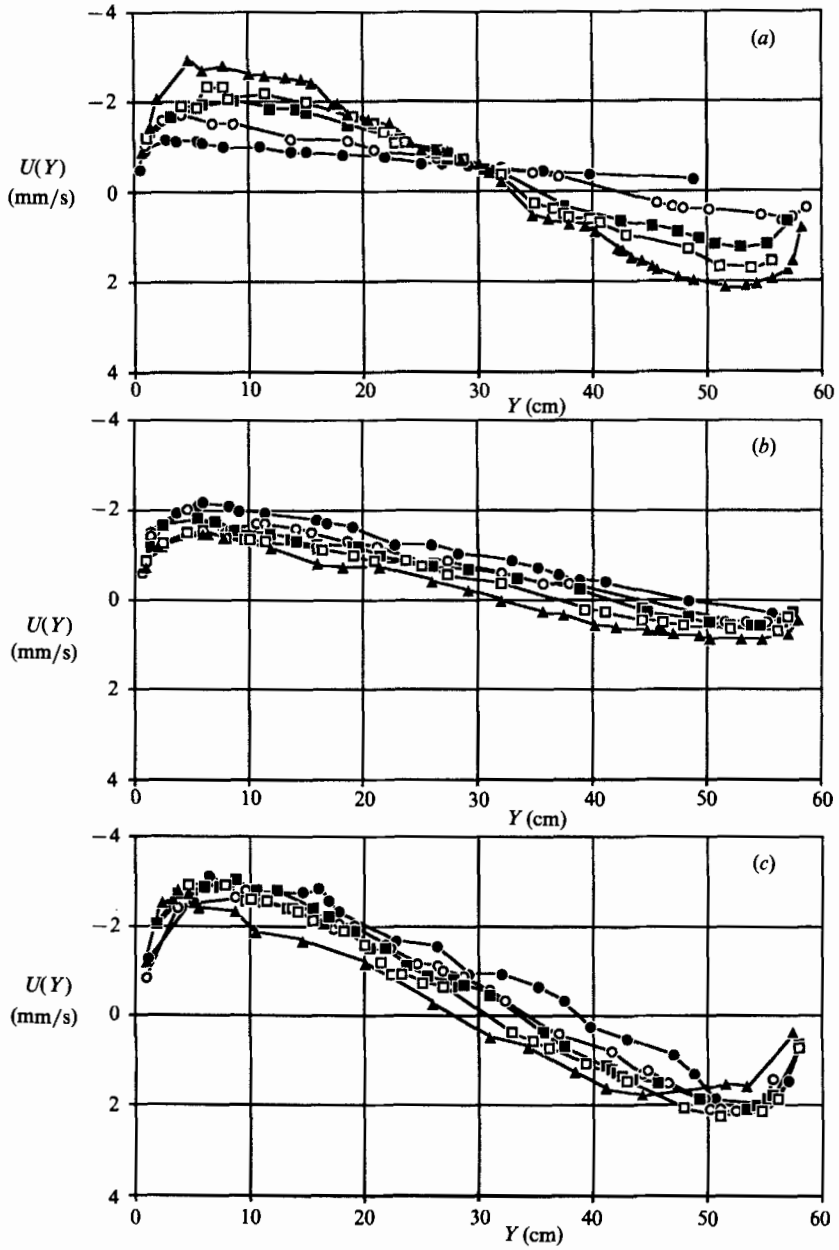

FIGURE 8. $U(Y)$ in exp. 9 at (*a*) $X = 162$ cm and $T = 60$ s (●), 300 s (○), 1445 s (■), 2225 s (□), 3600 s (▲). (*b*) $X = 50$ cm (●), 100 cm (○), 150 cm (■), 200 cm (□), 250 cm (▲) and $T = 600$ s. (*c*) $T = 3600$ s (the symbols are the same as those used in (*b*).

For example, a calculation based on the last profile in figure 8(*a*) gives ζ ($X = \frac{1}{2}L$, $Y = 0) \sim +0.84f$ at $T = 3600$ s. In most experiments (all except 1, 9 and 13), this boundary-layer vorticity appeared to lead to the breakup of the mean flow into the gyres seen, for example, in figure 5(*d*). This process of gyre formation can best be described as resulting from the separation of the main flow in the corners of the tank.

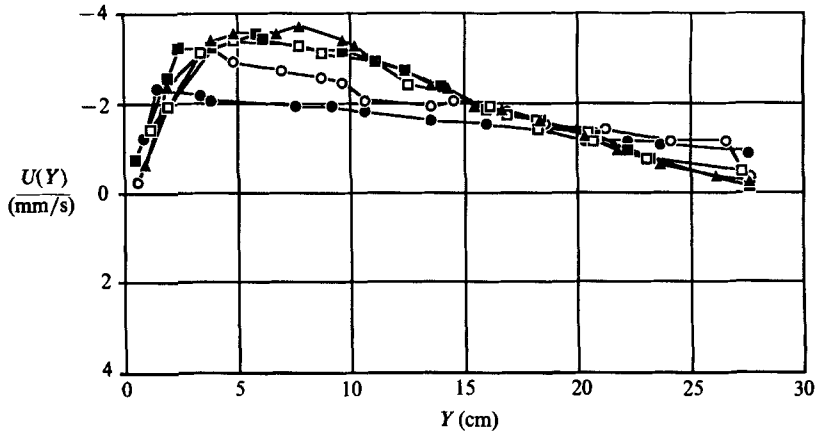

FIGURE 9. $U(Y)$ in exp. 13: $X = 162$ cm and $T = 60$ s (●), 300 s (○), 1200 s (■), 1800 s (□), 2700 s (▲).

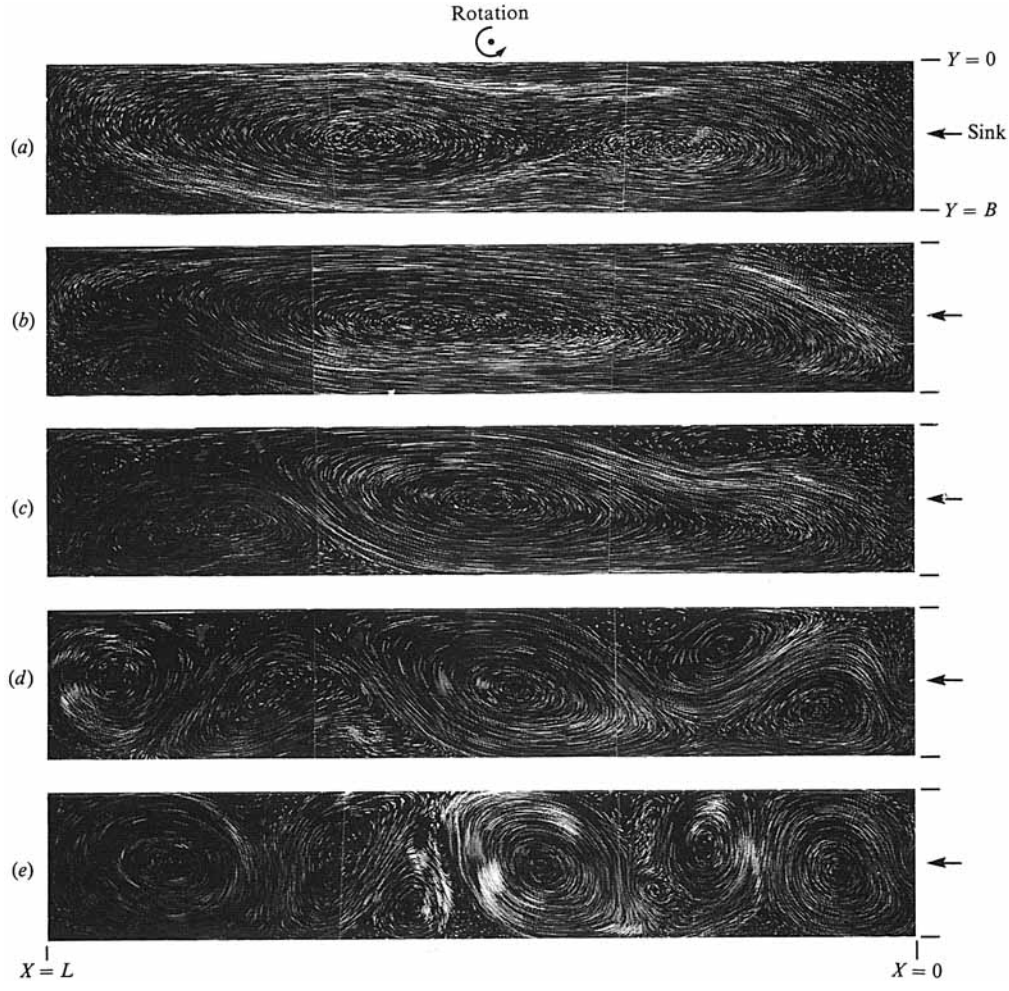

FIGURE 10. Breakdown of the withdrawal flow in exp. 7 ($S = 0.13$). The times are (*a*) 900 s, (*b*) 1245 s, (*c*) 1575 s, (*d*) 1800 s, (*e*) 2115 s.

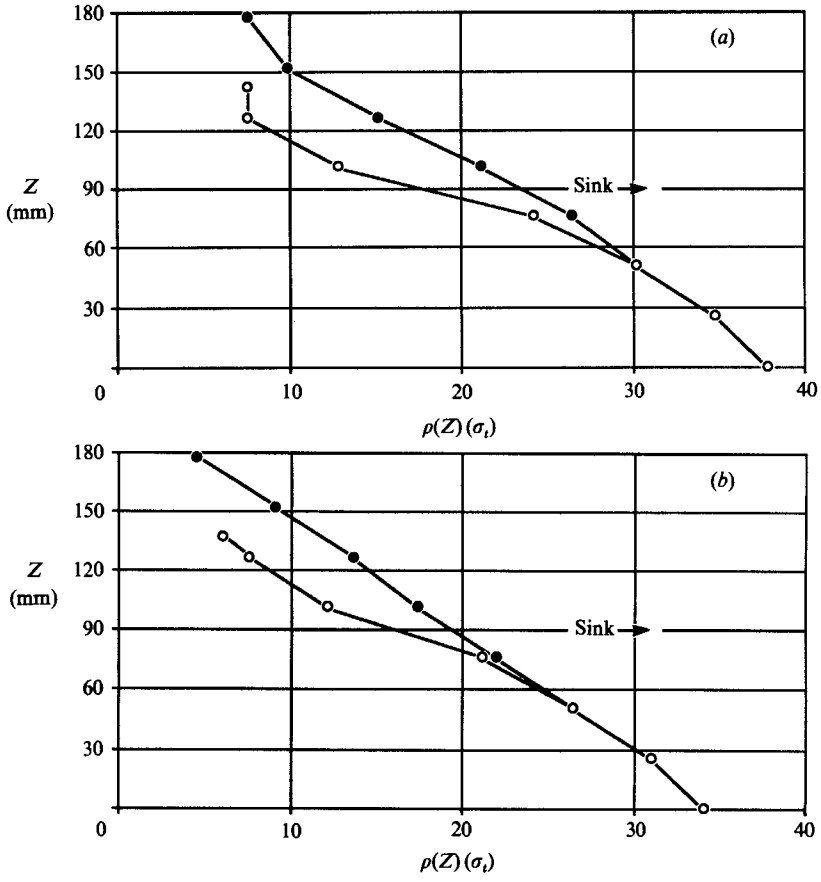

FIGURE 11. Density profiles in (*a*) exp. 11 ($S = 0.25$) and (*b*) exp. 13 ($S = 1.25$) taken before (●) and after (○) each experiment.

An example of this breakup of the mean flow is shown in figure 10, a sequence of photos taken in exp. 7 ($S = 0.13$). The first photo (10*a*) shows a general clockwise flow within which are embedded two clockwise vortices (remnants of the initial conditions); these were subsequently incorporated into the mean flow. The second photo (10*b*) shows the start of the breakup of the flow: the withdrawal current separates from the walls in the corners at $(X, Y) = (0, 0)$ and (L, B), forming two regions of positive vorticity. The sidewall boundary layers continue to feed positive vorticity into these regions, leading to the development of two counterclockwise vortices. Owing to induction (Batchelor 1967, p. 517 ff.), these vortices should migrate towards the centre of the tank; this migration is initially suppressed by the withdrawal flow, which acts to confine the vortices to the corners. However, when the vortices have attained sufficient strength (10*c*), their self-induced velocity is large enough to enable them to move against the withdrawal current towards the centre of the tank (10*d*), where they become established as counterclockwise gyres between alternate clockwise gyres (10*e*). Once nestled between clockwise gyres, the counterclockwise gyres are spun-up rapidly by the pinched-off withdrawal current that results. The resulting flow is quite similar in appearance to that observed in convection experiments (Hide & Mason 1975) or in stress-driven upwelling experiments (Narimousa & Maxworthy 1985), although the underlying dynamics of

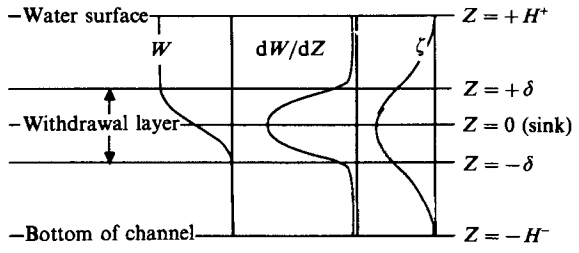

FIGURE 12. Definition sketch for the model problem.

the gyre formation, i.e. the process of boundary-layer separation, appears to be somewhat different than that which characterizes these other unstable rotating flows.

4.3. *Effect of fluid withdrawal on density structure*

The effect of withdrawal flows of this type on the density structure of the fluid in the tank is shown in figure 11, where we present pairs of density profiles taken before the pump was turned on and after it was turned off in exps 11 and 13. The shapes of these latter profiles are typical of withdrawal flows (Spigel & Farrant 1984) in that they show depletion of fluid below the level of the sink, and a nearly uniform downwards motion of fluid a short distance ($\approx \delta$) above the sink (as in the 'pack-of-cards' model discussed by Imberger *et al.* 1976). More specifically, Spigel & Farrant's measurements for a non-rotating selective withdrawal flow show clearly that the density field below the withdrawal layer, defined using the vertical profile of the horizontal velocity (see Ivey & Blake 1985), is unaffected by the withdrawal process.

In contrast, our measurements (with rotation) show that the withdrawal layer defined in terms of the vertical profile of the horizontal flow (which grew in vertical extent with time) was thicker than the withdrawal layer defined in terms of modification of the density field. Figure 11 shows that according to this latter definition, the withdrawal-layer thickness (δ) must have been less than 40 mm in both exps 11 and 13, i.e. it was not nearly as thick as the velocity profiles measured in either experiment lead us to believe. On the other hand, this density-based upper bound on δ is reasonably close to the value of δ (38 mm) we estimated using the *initial* velocity profiles.

5. A model of spin-up and its possible effects on withdrawal dynamics

5.1. *The model equation*

In this section we present a model of the experimentally observed spin-up process. In particular, we try to explain the mean features of our observations: the lack of horizontal variations in the vertical relative vorticity, ζ, except in the sidewall boundary layers and near the sink; and the fact that the values of (ζ/f) we observed at mid-depth in the experiments were in the range of -0.1 to -0.2, rather than attaining values much closer to -1.0 (the maximum possible). We consider the case where $(N/f) \gg 1$, so that stratification suppresses Ekman suction (Greenspan 1968) and, initially, the withdrawal-layer thickness is not affected by rotation. Once we have calculated ζ, we can then calculate the recirculating velocity field and finally, because the longitudinal flow is in geostrophic balance, the distortion of the density

field necessary to satisfy the thermal wind relation. The geometry of the problem is sketched in figure 12.

In non-rotating selective withdrawal, the vertical velocity is approximately independent of horizontal position when the Froude number, $Q/(NH^2B)$, is small enough (Imberger *et al.* 1976). Thus, the means by which negative vorticity can be created, vortex compression, is spatially uniform. If horizontal variations in ζ are small initially, they will tend to remain so. Thus we can use a one-dimensional advective–diffusion equation to model the evolution of ζ; the appropriate equation is

$$\partial_T \zeta + W\,\partial_Z \zeta - \nu \partial^2_{ZZ} \zeta - \zeta \frac{\mathrm{d}W}{\mathrm{d}Z} = f \frac{\mathrm{d}W}{\mathrm{d}Z}. \tag{10}$$

This equation should be valid for $T \sim T_\delta$ (see (9)). To solve (10) we must assume a form for W. According to Spigel & Farrant (1984),

$$\begin{aligned} W(Z) &= -(Q/2\delta A)\,((Z+\delta) + (\delta/\pi)\sin(\pi Z/\delta)), && -\delta \leqslant Z \leqslant +\delta \\ &= -(Q/A), && +\delta \leqslant Z \\ &= 0, && -\delta \geqslant Z, \end{aligned} \tag{11}$$

where Q is the volume flow rate, δ is half of the total withdrawal-layer thickness, and A is the surface area of the reservoir (for a rectangular geometry $A = BL$). Equation (11) implicitly defines δ in terms of modification of the density profile by vertical advection. The Z-axis is defined so that $Z = 0$ is the centre of the withdrawal layer. In order to isolate the flow associated with spin-up, we assume that $\zeta = 0$ at $T = 0$. On the no-slip bottom, $Z = -H^-$, $\zeta = 0$, and, to model the laboratory experiments, we also assume that $\zeta = 0$ at the free surface, $Z = H^+$ (because of surface films). In most of the results we shall discuss $H^+ = H^-$; this symmetrical placement of the sink corresponds to the initial conditions of all of our experiments. In order to model the asymmetry which we hypothesized was due to location of the free surface relative to the sink, we also considered a case in which $H^+ \neq H^-$.

A useful form of (10) is one written in terms of the non-dimensional variables (denoted by *):

$$\zeta = f\zeta^*, \quad T = T_\delta t^*, \quad Z = \delta z^*, \quad W = (Q/\delta A)\,w^*, \tag{12}$$

which reduces (10) to (dropping the *)

$$\partial_t \zeta + w\partial_z \zeta - Re^{-1}\partial^2_{zz}\zeta - \zeta \frac{\mathrm{d}w}{\mathrm{d}z} = \frac{\mathrm{d}w}{\mathrm{d}z}. \tag{13}$$

Equation (13) contains a single parameter,

$$Re = (Q\delta/\nu A). \tag{14}$$

Re is a Reynolds number based on the vertical velocity; it is also the ratio of the diffusion timescale (δ^2/ν) to T_δ. This scaling indicates that when $Re = O(1)$, none of the terms appearing in (11) can be omitted. Lastly, once (11) has been made dimensionless, the boundary conditions are applied at $z = \pm(H^\pm/\delta) = \pm\lambda^\pm$.

Equation (13) was solved numerically using a simple, explicit finite-difference scheme (centred differences, first-order in time) using a grid with nodes spaced 0.2 units apart. The time interval was chosen so as to satisfy the Courant–Friedrich–Lewy condition $(0.5\Delta z^2\,\Delta t^{-1} > Re^{-1})$ for the given node spacing (Dahlquist & Björk 1974). In order to keep the solution technique simple, it was impossible to

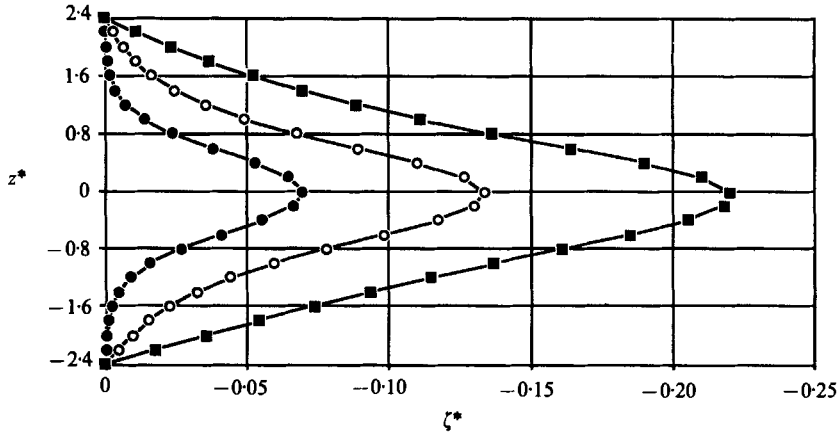

FIGURE 13. Calculated profiles of ζ, the dimensionless vertical vorticity for symmetrical boundaries. The symbols correspond to $t = 0.1$ (●), 0.3 (○), 0.9 (■).

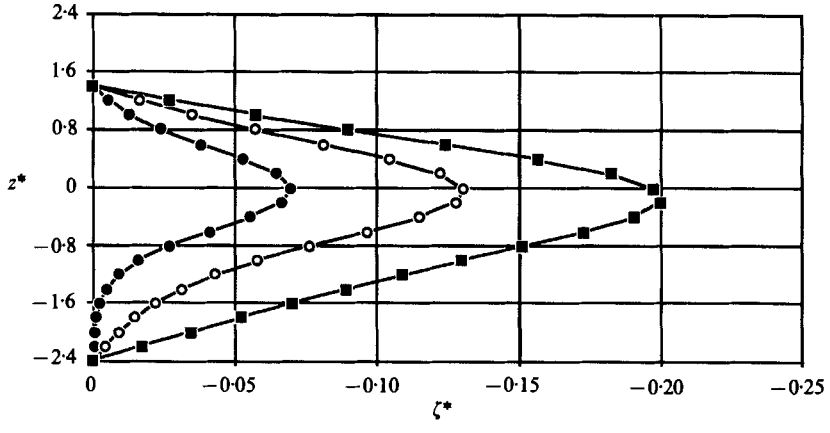

FIGURE 14. Calculated profiles of ζ, the dimensionless vertical vorticity for asymmetrical boundaries. The symbols correspond to $t = 0.1$ (●), 0.3 (○), 0.9 (■).

account for the fall of the free surface with time. This is equivalent to assuming that $\lambda^+ \gg 1$. We did attempt to qualitatively represent the effect of the free-surface position on the vorticity distribution by carrying out a calculation in which $\lambda^+ = 1.4$ while $\lambda^- = 2.4$. This would correspond to conditions existing in our tank when $t = 1$.

5.2. *Results*

Plots of calculated values of $\zeta(z)$ at different times for symmetrically placed boundaries are given in figure 13. The parameters chosen for the calculation, $\lambda^{\pm} = 2.4$ and $Re = 0.43$ are representative of the experimental conditions (based on the observed withdrawal-layer thickness of 38 mm and the initial depth) found in exps 10–13. Values of these two parameters appropriate to the rest of the experiments are reasonably similar to those used in the numerical solution; therefore, the behaviour shown in figure 13 should be qualitatively similar to that which would be calculated for all of the experiments.

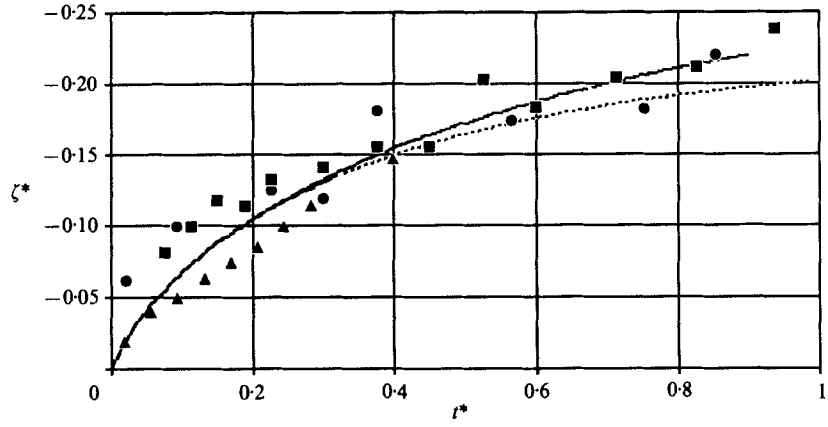

FIGURE 15. A comparison of calculated (solid line = symmetric, dotted line = asymmetric) and measured values of the dimensionless vertical vorticity $\zeta(z = 0, t)$ in exps 11 (●), 10 (○), 13 (■).

The profiles of ζ given in figure 13 show that withdrawal-layer vorticity increases with time and diffuses vertically. Evidently, diffusion is sufficiently strong that the vorticity distribution remains nearly symmetric about $z = 0$, rather than showing significantly larger values of ζ in the lower part of the withdrawal layer. The reason we suggest any asymmetry for symmetrically placed boundaries is that above $z = 0$ there is downwards advection of less spun-up fluid whereas below $z = 0$ there is downwards advection of more spun-up fluid. In terms of (13), w ($\mathrm{d}\zeta/\mathrm{d}z$) is negative above the sink and retards the local spin-up of vorticity, whereas it is positive below the sink, and thus aids the local spin-up process. Although the calculated profiles are nearly symmetric in this case, advection cannot be neglected: simpler versions of (13) that neglect $w\partial_z\zeta$ give somewhat larger values of ζ than when it is included.

This diffusive behaviour of the withdrawal flow is similar to that observed by Kranenburg (1980) in his experiments with an homogeneous layer overlying a linearly stratified layer. Because he withdrew fluid from the homogeneous layer, there was no direct spin-up of the stratified region; instead, spin-up there was due entirely to diffusion.

The results of the calculation made with asymmetrically placed boundaries is shown in figure 14. Here again, the effects of diffusion are quite strong. Initially the profiles are nearly symmetrical about $z = 0$, but, because of the placement of the upper boundary, the distribution of ζ has become quite asymmetric by the time $t \approx 0.9$. Since the horizontal velocity is proportional to ζ (see (16) below), we can directly compare the shapes of these profiles of ζ with the profiles of $U(Z)$ given in figure 3. In spite of the simplicity of the model, this comparison is quite good, indicating that the observed asymmetry is due to the location of the free surface relative to the level of the sink.

The time dependence of the spin-up process is shown in figure 15, in which we compare theoretical (both cases) and experimental values of $\zeta(z = 0, t)$ obtained from the bead-streak data. This comparison between experiment and theory is quite good. Because the theory does not account for the shear set up by the initial Kelvin waves, the observed values of ζ are larger than their theoretical counterparts at the outset of each run. However, this initial vorticity retards the spin-up (this is the effect of the term ζ ($\mathrm{d}w/\mathrm{d}z$) in (13)), so that as t increases, the observed values of ζ approach (from

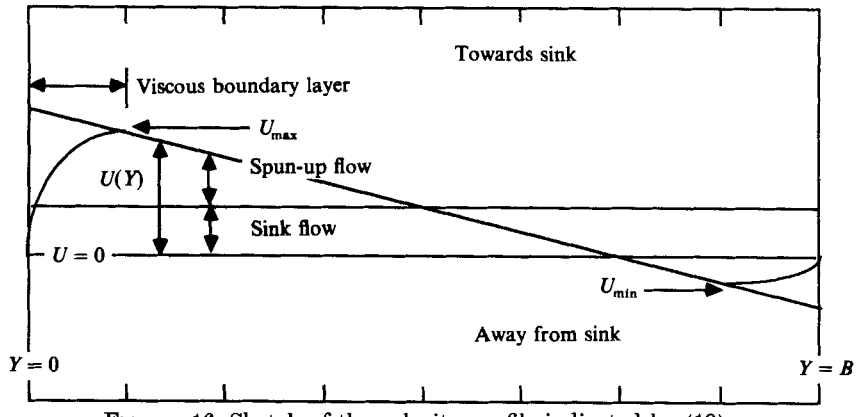

FIGURE 16. Sketch of the velocity profile indicated by (19).

above) the calculated curve. Note also that the two theoretical curves are virtually indistinguishable until $t \approx 0.4$, and only differ by about 10% when $t \approx 1$.

Most importantly, there is no systematic deviation of the observations from the calculated curve although there is a factor of 4 difference in S among the three sets of experimental points plotted in figure 14. If δ (appearing in (10)) had increased with time because of rotation, as Whitehead (1980) suggests, ζ would have increased more slowly than if δ had remained constant. Thus, the agreement of theory and observations lends further weight to our suggestion that for rotating selective withdrawal, it is important to distinguish between the withdrawal layer defined in terms of advective modification of the density profile and that which is defined in terms of the horizontal flow induced by the outflow in the presence of rotation.

5.3. *The spun-up velocity field*

Once we know ζ, we can solve for the induced flow. We have two equations for U and V (returning to dimensional variables):

$$\partial_X U + \partial_Y V = -\frac{\mathrm{d}W}{\mathrm{d}Z}, \tag{15a}$$

$$\partial_Y U - \partial_X V = \zeta(Z,T), \tag{15b}$$

where W and ζ are known functions of Z and T. A solution to this set of equations, appropriate to a line sink, or a point sink for $(x/B) > 1$ (Spigel & Farrant 1984), is

$$U = (\partial_Y \Psi)\zeta + \frac{\mathrm{d}W}{\mathrm{d}Z}(L-X), \tag{16a}$$

$$V = (-\partial_X \Psi)\zeta, \tag{16b}$$

where

$$\nabla^2 \Psi = 1 \tag{17}$$

subject to the boundary condition that

$$\Psi = 0$$

on the boundary of the tank. By elementary methods, we find that

$$\Psi = \sum_{\substack{m=1 \\ \text{(both odd)}}}^{\infty} \sum_{n=1}^{\infty} \frac{16L^2B^2}{nm\pi^2}(m^2\pi^2B^2 + n^2\pi^2L^2)^{-1} \sin\frac{m\pi X}{L} \sin\frac{n\pi Y}{B}. \tag{18}$$

By neglecting X-variations in the flow, a simpler solution is obtained; i.e. by making a boundary-layer-type approximation to flow variations, (15) can be integrated to give

$$U = (Y - \tfrac{1}{2}B)\,\zeta + \frac{\mathrm{d}W}{\mathrm{d}Z}(L - X). \tag{19}$$

Equation (19) describes a flow that is the superposition of a linear shear flow and a two-dimensional sink flow. The sink flow is identical to that which would be found in the absence of rotation for a line sink; the flow into a point sink (the experimental configuration) would differ from that into a line sink only for $X < B$ (Spigel & Farrant 1984). The velocity field represented by (19) is sketched in figure 16 (where we have also added in sidewall boundary layers schematically). The similarity between the shape of the velocity profile sketched in figure 16 and the shapes of the experimental curves plotted in figures 8 and 9 is striking, and suggests that the model provides a reasonable description of a flow observed prior to the onset of the instability seen in figure 10.

5.4. *Modifications of the density field by spin-up*

The velocity field described by (19) requires that the density field become distorted in the (Y, Z)-plane in order to prevent the Coriolis force (fU) from accelerating a transverse flow (V). Here we examine whether or not this deformation is comparable to δ. A scale analysis shows that the lowest-order Y-momentum equation is the so-called thermal wind equation (e.g. Gill 1982)

$$f\,\partial_Z U = -N^2 \frac{\mathrm{d}\eta}{\mathrm{d}Y}, \tag{20}$$

where $\eta(Y, Z, T)$ is the displacement of an isopycnal surface from its level position. Thus

$$\frac{\mathrm{d}\eta}{\mathrm{d}Y} = -\frac{f}{N^2}\left\{(Y - \tfrac{1}{2}B)\,\partial_Z \zeta + \frac{\mathrm{d}^2 W}{\mathrm{d}Z^2}(L - X)\right\}. \tag{21}$$

We can drop the second term on the right-hand side of (21) because it is much smaller than the first term (the ratio of the two terms is $\sim Q(f\delta B^2)^{-1} \ll 1$). Therefore, integrating (21) with respect to Y, using the condition

$$\int_0^B \eta \,\mathrm{d}Y = 0, \tag{22}$$

we find

$$\eta = -\frac{f}{2N^2}\partial_Z \zeta (Y^2 - BY + \tfrac{1}{6}B^2). \tag{23}$$

According to (23), the maximum isopycnal displacements ($|\eta|$) occur at $Y = 0, B$ (the walls) and at the depth where $|\partial_Z \zeta|$ is maximum. For example, we find from figure 13 that the maximum value of $\partial_Z \zeta \approx 0.15(f/\delta)$ at $T/T_\delta \approx 0.75$. Thus, the maximum value of η, normalized by δ is (for the experimental parameters)

$$(\eta/\delta)_{\max} \approx 8.3 \times 10^{-3} S^{-2}.$$

That is, for experiments 10, 11 and 13 we find that $(\eta/\delta)_{\max}$ ranges from 2.3×10^{-2} to 5×10^{-3}. Thus, the spun-up flow only slightly distorts the density field, and thus does not suppress spin-up or alter withdrawal dynamics in the sense of thickening the withdrawal layer.

6. Discussion and conclusions

Our experimental results can be summarized as follows: when the sink is switched on, Kelvin shear waves are generated which propagate around the perimeter of the tank setting up an anticyclonic selective-withdrawal current. Owing to the compression of filaments of planetary vorticity in the withdrawal layer (albeit moderated by vertical diffusion of vorticity) this withdrawal current accelerates so that the vertical vorticity is nearly uniform in any horizontal plane. Triggered by boundary-layer separation, this shear flow eventually breaks down, leading to a state wherein the withdrawal current is confined to a narrow jet threading its way between counter-rotating gyres each having a diameter roughly equal to the width of the tank.

Both a qualitative analysis of the initial setting up of the withdrawal layer, and a simple analytical model of the spin-up process, suggest that S, the Burger number defined using the withdrawal-layer shear-wave speed, is a useful measure of the effects of rotation on selective withdrawal. As seen in our experiments, the chief differences among flows having different values of S are the scale of decay of the initial velocity field (i.e. the Rossby radius of the initial flow) and the relative strengths of the sinkwards flow and the recirculating flow.

The latter difference really reflects the dependence of the flow on one other parameter. If we consider the ratio of the withdrawal current, $U_w \sim Q(\delta B)^{-1}$ to the recirculating current $U_r \sim fB$, we arrive at a new Rossby number,

$$Ro_Q = Q(f\delta B^2)^{-1} \tag{24}$$

which measures the relative strengths of the two flows. For a point sink we can express Ro_Q in terms of S, viz. $Ro_Q = (\delta/B)S$. Because $(\delta/B) \ll 1$, we find that $Ro_Q < 1$, even if $S > 1$.

A comparison of velocity and density-field data shows that the withdrawal layer defined by the velocity field thickens with time and, soon after the start of the experiments, is thicker than the withdrawal layer defined by advective changes in the density profile. In terms of this latter basis for defining δ, our data do not show any thickening of the withdrawal layer due to rotation. Indeed, the analysis given in §5 leads us to conclude that the thickening of the velocity-based withdrawal profile was due entirely to diffusion of the relative vertical vorticity created in the collapsing withdrawal layer.

The reasons why rotation might not influence the density-based withdrawal-layer thickness are best seen by considering several possible scalings that attempt to find the relationship between withdrawal-layer thickness and rotation rate. First, consider the analysis given by Imberger & Hamblin (1982). They assume a 'thermal-wind' balance based upon steady-state conditions and solve for δ and b, the current thickness and width. Setting $U \sim N\delta$, and then balancing the transverse pressure gradient and Coriolis force, they find

$$b \sim QN\delta^2. \tag{25}$$

implying that

$$\delta \sim (f/N)^{\frac{1}{3}}(Q/N)^{\frac{1}{3}}. \tag{26}$$

However, if the outlet is a point sink, the withdrawal layer must have at least a thickness $\sim(Q/N)^{\frac{1}{3}}$ (for an inertial flow), so that unless $(f/N) \sim 1$, the isopycnal displacements due to rotation will be less than those required by inertia. Hence,

following Imberger & Hamblin's argument, rotation will not affect the layer thickness unless $(f/N) \sim 1$. Given that $f \sim 10^{-4}\,\mathrm{s}^{-1}$ in many environmental applications, the preceding condition restricts their analysis to weak stratifications only.

An alternative view, one ignoring the spin-up process, is to assume a slight transverse deflection η that is superimposed on a pre-existing withdrawal structure. Again balancing the transverse pressure gradient and the Coriolis force, assuming an unknown transverse lengthscale b, and estimating the perturbation pressure as

$$P \sim \rho N^2 \delta \eta,$$

as estimate for η when the outlet is a point sink is

$$\eta \sim (f/N)\,(Q/N)^{\frac{1}{3}} \sim (f/N)\,\delta. \tag{27}$$

Thus before spin-up, the transverse isopycnal displacements are much smaller than the layer thickness. Furthermore, confirming Gill's (1976) analysis, the arguments leading to (27) do not allow us to estimate b through consideration of a steady momentum balance. Instead, the width of the withdrawal current is set by the superposition of several Kelvin-wave velocity fields, each having its own characteristic transverse lengthscale; i.e. b is determined by an unsteady momentum balance.

Last, we consider the fully spun-up flow for which $\partial_z \zeta \sim (f/\delta)$, implying

$$(\eta/\delta) \sim (f^2 B^2)/(N^2 \delta^2) = S^{-2}. \tag{28}$$

Thus, the Burger number, S, not only measures the importance of rotation in determining the establishment of the flow, it also measures the relative distortion of the density field by inertial and rotational effects. However, because of the small constant of proportionality (e.g. 8×10^{-3} in the present case), only when $S \ll 1$ are isopycnal displacements, and hence (possibly) withdrawal-layer thicknesses, larger than in the non-rotating case.

To put our study into perspective, it is useful to calculate S, Re and Ro_Q for prototype flows. For a medium-size reservoir, $B \sim 500$ m, $\delta \sim 5$ m, $Q \sim 1\ \mathrm{m}^3\,\mathrm{s}^{-1}$, $f \sim 10^{-4}\,\mathrm{s}^{-1}$, $N \sim 10^{-2}\,\mathrm{s}^{-1}$, and $\nu = 10^{-4}\,\mathrm{m}^2\,\mathrm{s}^{-1}$; we calculate $S \sim 1$, $Re = 0.02$, and $Ro_Q = 0.01$. Thus we conclude that in the absence of other influences, the flow would spin-up in a manner similar to that observed in our experiments; given enough time (which for $L \sim 5$ km, would be $T_\delta \sim 100$ days), we expect that those currents induced by rotation would eventually exceed those due to withdrawal alone.

This study forms a part of the CWR Canning Reservoir Study carried out for the Water Authority of Western Australia and was also partially supported by the Australian Research Grants Scheme Grant F8415255 to UWA and by the Office of Naval Research Grant N00014-82-K-0084 to USC. The first author gratefully acknowledges additional assistance provided him by the Department of Civil Engineering and the School of Engineering at Stanford University. An earlier version of this paper was presented at the Third Stratified Flow Symposium held in February 1987. The authors are grateful to Drs J. Patterson, G. Lawrence, S. Narimousa, and G. Spedding, for their help with this study, and to J. Koseff and G. Schladow for their comments concerning a draft of this paper.

REFERENCES

BATCHELOR, G. K. 1967 *An Introduction to Fluid Dynamics*. Cambridge University Press.

BUZYNA, G. & VERONIS, G. 1971 Spin-up of a stratified fluid: theory and experiment. *J. Fluid Mech.* **50**, 579–608.

DAHLQUIST, G. & BJÖRK, A. 1974 *Numerical Methods*. Prentice Hall.

GILL, A. E. 1976 Adjustment under gravity in a rotating channel. *J. Fluid Mech.* **77**, 603–621.

GILL, A. E. 1982 *Atmosphere-Ocean Dynamics*. Academic.

GREENSPAN, H. P. 1968 *The Theory of Rotating Fluids*. Cambridge University Press.

HIDE, R. & MASON, P. J. 1975 Sloping convection in a rotating fluid. *Adv. Phys.* **24**, 47–100.

IMBERGER, J. 1980 Selective withdrawal: a review. *IAHR Proc. Second Intl Symp. on Stratified Flows, Trondheim, Norway*, vol. 1, pp. 381–400.

IMBERGER, J. & HAMBLIN, P. F. 1982 Dynamics of lakes, reservoirs, and cooling ponds. *Ann. Rev. Fluid Mech.* **14**, 153–187.

IMBERGER, J., THOMPSON, R. O. R. Y. & FANDRY, C. 1976 Selective withdrawal from a finite rectangular tank. *J. Fluid Mech.* **70**, 489–512.

IVEY, G. N. & BLAKE, S. 1985 Axisymmetric withdrawal and inflow in a density-stratified container. *J. Fluid Mech.* **161**, 115–137.

KRANENBURG, C. 1980 Selective withdrawal from a rotating two-layer fluid. *IAHR Proc. Second Intl Symp. on Stratified Flows, Trondheim, Norway*, vol. 1, pp. 401–410.

LAWRENCE, G. A. 1980 Selective withdrawal through a point sink. *Proc. Second Intl Symp. on Stratified Flows, Trondheim, Norway*, vol. 1, pp. 411–423.

MAXWORTHY, T. 1983 Experiments on solitary internal Kelvin waves. *J. Fluid Mech.* **129**, 365–383.

MAXWORTHY, T. & BROWAND, F. K. 1975 Experiments in rotating and stratified flows: oceanographic application. *Ann. Rev. Fluid Mech.* **7**, 273–305.

NARIMOUSA, S. & MAXWORTHY, T. 1985 Two-layer model of shear-driven coastal upwelling in the presence of bottom topography. *J. Fluid Mech.* **159**, 503–531.

PAO, H. P. & KAO, T. W. 1974 Dynamics of establishment of selective withdrawal of a stratified fluid from a line sink. Part 1. Theory. *J. Fluid Mech.* **65**, 657–688.

PATTERSON, J. C., HAMBLIN, P. F. & IMBERGER, J. 1984 Classification and dynamics of the vertical density structure of lakes. *Limnol. Oceanogr.* **29**, 845–861.

SILVESTER, R. 1978 An experimental study of end-wall effects on selective withdrawal from a reservoir. PhD thesis, Department of Mechanical Engineering, University of Western Australia.

SPIGEL, R. H. & FARRANT, B. 1984 Selective withdrawal through a point sink and pycnocline formation in a linearly stratified flow. *J. Hydraul. Res.* **22**, 35–51.

WHITEHEAD, J. A. 1980 Selective withdrawal of a rotating stratified fluid. *Dyn. Atmos. Oceans* **5**, 123–135.